# In Vivo Model for Evaluating the Effects of Mechanical Stimulation on Tissue-Engineered Bone Repair

**Joel D. Boerckel**

**Kenneth M. Dupont**

G. W. Woodruff School of Mechanical Engineering,
Georgia Institute of Technology,
315 Ferst Drive,
Atlanta, GA 30332

**Yash M. Kolambkar**
W. H. Coulter Department of Biomedical Engineering,
Georgia Institute of Technology,
315 Ferst Drive,
Atlanta, GA 30332

**Angela S. P. Lin**
G. W. Woodruff School of Mechanical Engineering,
Georgia Institute of Technology,
315 Ferst Drive,
Atlanta, GA 30332

**Robert E. Guldberg**
G. W. Woodruff School of Mechanical Engineering,
and W. H. Coulter Department of Biomedical Engineering,
Georgia Institute of Technology,
315 Ferst Drive,
Atlanta, GA 30332
e-mail: robert.guldberg@me.gatech.edu

*It has long been known that the bone adapts according to the local mechanical environment. To date, however, a model for studying the effects of functional mechanical loading on tissue-engineered bone repair in vivo has not yet been established. We have developed a rat femoral defect model, in which ambulatory loads are transduced through the implanted tissue-engineered construct to elucidate the role of the mechanical environment in functional restoration of a large bone defect. This model uses compliant fixation plates with integrated elastomeric segments, which allow transduction of ambulatory loads. Multiaxially and uniaxially compliant plates were characterized by mechanical testing and evaluated using in vivo pilot studies. In the first study, experimental limbs were implanted with multiaxial plates, which have a low stiffness in multiple loading modes. In the second study, experimental limbs were stabilized by a uniaxial plate, which allowed only axial deformation of the defect. X-ray scans and mechanical testing revealed that the multiaxial plates were insufficient to stabilize the defect and prevent fracture under ambulatory loads as a result of low flexural and torsional stiffness. The uniaxial plates, however, maintained integrity of the defect when implanted over a 12 week period. Postmortem microCT scans revealed a 19% increase in bone volume in the axially loaded limb compared with the contralateral standard control, and postmortem mechanical testing indicated that torsional strength and stiffness were increased 25.6- and 3.9-fold, respectively, compared with the control. Finite element modeling revealed high strain gradients in the soft tissue adjacent to the newly formed bone within the implanted construct. This study introduces an in vivo model for studying the effects of physiological mechanical loading on tissue-engineered bone repair. Preliminary results using this new in vivo model with the uniaxially compliant plate showed positive effects of load-bearing on functional defect repair.* [DOI: 10.1115/1.3148472]

*Keywords: bone, tissue engineering, mechanical stimulation, biomechanics*

## 1 Introduction

Living systems exhibit remarkable plasticity in the face of mechanical stimuli. Biomechanical factors influence nearly every stage of life including the growth, development, maintenance, degeneration, and repair of most tissues. A growing knowledge of the mechanisms by which living organisms adapt to the local mechanical environment is advancing the potential for tissue engineers to restore, maintain, and improve tissue function [1]. Stimulatory mechanical loading has been shown to enhance the properties of many types of engineered tissues including cartilage, ligament, muscle, and blood vessels [2]. Bone is also known to be highly adaptive. Normal bone adapts and remodels in a highly regulated fashion [3]. Extensive research has also shown the fracture healing process to be acutely sensitive to mechanics, with moderate level compressive strains being anabolic to callus formation and new bone deposition [4]. The role of mechanical loading in functional integration of tissue-engineered constructs implanted into large bone defects, however, has not yet been studied.

The restoration of function to large bone defects caused by traumatic bone injury, tumor resection, or degenerative bone disease is a significant clinical challenge, with particular interest lately due to the extent of complex limb injuries sustained by war victims [5]. Structural allografts represent the current clinical standard for defects greater than 3 cm but are slow to revascularize and remodel and have a high rate of failure due to fracture [6]. Tissue-engineered constructs combining biomaterial scaffolds and biologics, such as growth factors or osteoprogenitor cells, are therefore a promising alternative. However, the effects of physiological loading on construct integration, tissue remodeling and restoration of long bone function are not well understood.

Bioreactors and other in vitro systems are becoming increasingly common, but a platform model to investigate the effects of mechanical stimuli on functional integration of tissue-engineered constructs and subsequent bone repair in vivo has not yet been established. Such a platform model is necessary to determine the effects of mechanical stimuli on outcomes that cannot be adequately analyzed in vitro. Such effects include the survival and osteogenic differentiation of implanted stem cells, scaffold degradation kinetics, the inflammatory response that directs revascularization, and tissue remodeling, all of which may affect the rate and success of bone repair. Understanding these interactive effects would contribute to the better design of tissue-engineered constructs for clinically relevant loading conditions, help determine optimal fixation techniques for challenging segmental defect repair, and ultimately improve the clinical feasibility of tissue engineering-based strategies.

Here presented is the development of a rat femoral defect model in which ambulatory loads are transduced through the implanted tissue-engineered construct to elucidate the role of the mechanical environment in functional restoration of a large bone defect. Characterization of fixation plate response is evaluated through in vitro mechanical testing under multiple loading modes,

Contributed by the Bioengineering Division of ASME for publication in the JOURNAL OF BIOMECHANICAL ENGINEERING. Manuscript received October 13, 2008; final manuscript received March 16, 2009; published online July 2, 2009. Review conducted by Michael Sacks.

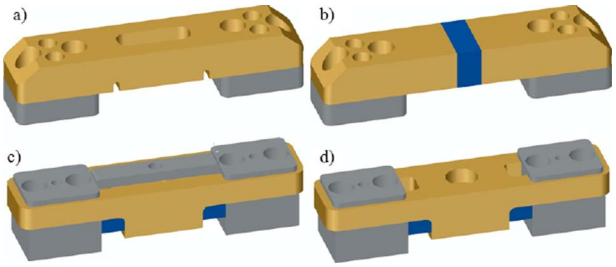


**Fig. 1 Fixation plate designs: (*a*) standard plate, (*b*) multiaxially compliant plate, (*c*) unactuated uniaxially compliant plate, and (*d*) actuated uniaxially compliant plate. Removal of the rigid clip actuates the uniaxial plate, allowing load transduction through the elastomer.**

and two pilot studies are presented, which demonstrate the ability to monitor defect stability and to quantify subsequent functional regeneration under multiaxial and uniaxial load.

## 2 Methods

**2.1 Scaffold Production.** Poly(L-lactide-*co*-D,L-lactide 70:30)/tri-calcium phosphate (PLDL-TCP) scaffolds were produced with longitudinally-oriented porous microarchitecture, as previously described [7]. Briefly, 100 $\mu$m diameter removable fibers coated with medical grade PLDL combined with 10% TCP, by weight, and the porogen azodicarbonamide was used to create longitudinal pores, followed by decomposition of the porogen at 260°C resulting in a random microporosity. The scaffolds were cut to size (4 mm diameter$\times$8 mm length with 1.5 mm diameter core) and sterilized by gamma irradiation (2.5 Mrad).

**2.2 Growth Factor Loading.** Each scaffold was coated with 25 $\mu$g/mL rat plasma fibronectin (F0635; Sigma-Adlrich, St. Louis, MO) to improve cellular adhesion, and then loaded with recombinant human bone morphogenetic protein 2 (BMP-2) (355-BM/CF, R&D Systems, Minneapolis, MN) using a previously described protocol [8]. Briefly, the protein was reconstituted in 2% alginate functionalized with two G4RGDSP amino acid sequences per chain (RGD-alginate), and was pipetted into the scaffold and crosslinked by bathing in $CaCl_2$. Each scaffold received a volume of 50 $\mu$L of RGD-alginate containing 2 $\mu$g BMP-2.

**2.3 Surgical Procedure.** Using a previously described method [8], critically-sized (8 mm) bilateral segmental defects were created in the femora of 13 week old female SASCO-Sprague Dawley rats (Charles River Labs, Wilmington, MA) under isoflurane anesthesia. The growth factor-loaded polymer scaffolds were press-fitted into the defects, and the limbs were stabilized by either rigid or compliant fixation plates attached directly to the bone. Animals were given subcutaneous injections of 0.04 mg/kg buprenorphine every 8 h for the first 48 h postoperative (post-op) and 0.013 mg/kg every 8 h for the following 24 h. All procedures were reviewed and approved by the Institutional Animal Care and Use Committee at the Georgia Institute of Technology (Protocol No. A08032).

**2.4 Compliant Fixation Plate Development.** To achieve load transfer from the plate to the construct, the standard plates described previously [8] were first modified by incorporating a full-thickness segment of silicone elastomer (RTV Silicone Adhesive, Factor II, Inc., Lakeside, AZ) (Figs. 1(*a*) and 1(*b*)). This design was multiaxially compliant, possessing a low stiffness in response to multiple loading modes—axial, bending, torsion, and shear. A second design allowed only axial deformation of the defect under ambulatory loads by constraining the stainless steel plates, which were fixed to the bone to slide with respect to the polysulfone plate bridging the defect (Figs. 1(*c*) and 1(*d*)). A finite axial stiffness was effected by incorporating the silicone elastomer between the steel and polysulfone plates. A removable stainless steel clip served as a locking system that allowed elective actuation of load-sharing.

In the first study, femurs were stabilized by the standard fixation (std.) plate described previously. In experimental limbs, the standard plates were replaced in a second surgery at 8 weeks post-op with the multiaxially compliant (multi.) plates.

In the second study, experimental limbs were stabilized by the axially compliant (axial) plates. At the time of implantation, the axial plates were constrained to prevent motion and were actuated at week 4 postimplantation by surgical removal of the clip.

**2.5 Fixation Plate Mechanical Characterization.** Characterization of axial, flexural, and torsional plate stiffnesses was performed by affixing the plates to age-matched excised femurs and potting the epiphyses in Wood's metal (Alfa Aesar, Ward Hill, MA). Axial tests were conducted with and without a hydrated scaffold placed in the defect, and were performed under displacement control at a rate of 0.01 mm/s to a displacement of 1 mm. Torsional tests were conducted under angular displacement control to a rotation of $\pm$5 deg at a rate of 0.1 deg. Finally, three-point bending tests were conducted for the standard and axially-compliant plates under displacement control to a maximum deflection of 0.5 mm at a rate of 0.02 mm/s. The multiaxially compliant plates were tested in four-point bending to a maximum displacement of 1 mm at a rate of 0.05 mm/s. Standard beam bending theory was used to calculate the average flexural stiffness of each plate from the recorded loads and deflections.

**2.6 Faxitron and Postmortem MicroCT.** Longitudinal two-dimensional digital X-ray scans (Faxitron MX-20 Digital; Faxitron X-ray Corp., Wheeling, IL) were taken at 1 week, 4 weeks, 8 weeks, and 12 weeks postimplantation with an exposure time of 15 s and a voltage of 25 kV to provide a qualitative assessment of healing and defect bridging. At 12 weeks post-op, the animals were euthanized by $CO_2$ asphyxiation, and the femurs were excised for quantitative microCT scans (Viva-CT 40; Scanco Medical, Basserdorf, Switzerland) as described previously [8]. Scans were performed at medium resolution and 21 $\mu$m isometric voxel size with the scanner set at a voltage of 55 kVp and a current of 109 $\mu$A. Newly-formed bone was segmented from scaffold material and soft tissues using a global threshold corresponding to 272 mg hydroxyapatite/cm$^3$, and a Gaussian filter (sigma=1, support=1) was used to suppress noise. The volume of interest (VOI) selected for quantitative analysis was the central 333 slices (approximately 7.0 mm).

**2.7 Post-Mortem Biomechanical Analysis.** Following post-mortem microCT scans, femora were biomechanically tested in torsion to failure as described previously [9]. Briefly, the femora were cleaned of soft tissues and the ends were potted in Wood's metal. Samples were mounted in an ELF 3200 (Bose EnduraTEC, Minnetonka, MN) with custom fixtures. The modular design of the fixation plates allows removal of the plates without removing the bone screws, minimizing disruption of the defect. Following fixation plate removal, each sample was tested in torsion to failure at a rotation rate of 3 deg/s. Torsional stiffness and maximum torque at failure were recorded for each sample.

**2.8 Finite Element Modeling.** MicroCT image-based finite element (FE) models of the defect and ingrown tissues at four weeks post-op were created to predict tissue-level stress and strain distributions resulting from estimated ambulatory loads. One animal was sacrificed at four weeks post-op and a femur was excised, mechanically tested in axial compression, and scanned at medium resolution with an isometric voxel size of 21 $\mu$m. Images thresholded for both bone and soft tissues/scaffold material were concatenated, and then voxels were converted directly to finite elements. By assigning the newly-formed bone a local modulus of $E_{bone}$=2 GPa and comparing the effective axial stiffness of the

Table 1 Fixation plate mechanical characterization. All values are given as mean ± std. deviation.

| | Standard plate | Multiaxial plate | Uniaxial plate | |
|---|---|---|---|---|
| | | | Actuated | Unactuated |
| Axial stiffness ($k$) without scaffold (N/mm) | $214.3 \pm 4.1$ | $9.58 \pm 2.95$ | $8.4 \pm 0.4$ | $349.5 \pm 35.1$ |
| Axial stiffness ($k$) with scaffold (N/mm) | $256.3 \pm 32.8$ | $93.6 \pm 18.8$ | $87.0 \pm 28.3$ | $404.9 \pm 60.3$ |
| Torsional stiffness ($GJ/L$) (kN m/deg) | $14.8 \pm 1.61$ | $0.802 \pm 0.133$ | $6.95 \pm 0.18$ | $9.14 \pm 2.94$ |
| Flexural rigidity ($EI$) concave (N mm$^2$) | $29236.3 \pm 260.8$ | $146.3 \pm 50.4$ | $25688.3 \pm 657.4$ | $26938.7 \pm 629.5$ |
| Flexural rigidity ($EI$) convex (N mm$^2$) | $30472.0 \pm 736.8$ | $132.0 \pm 29.0$ | $28015.0 \pm 2076.1$ | $42392.0 \pm 8350.1$ |

model to the measured value determined by mechanical testing of that same femur, the soft tissue and scaffold modulus, $E_{st}$, could be estimated.

## 3 Results

**3.1 Fixation Plate Characterization.** Mechanical characterization of the plates revealed that the axial compressive stiffness of the standard plates was $214.3 \pm 4.1$ N/mm (mean ± std. dev.) (Table 1). With a hydrated scaffold placed in the defect to approximate the day-zero mechanical environment, the effective stiffness increased by 19%. The axial stiffnesses of the multiaxial and actuated uniaxial plates were 3.9% and 4.5% of the standard plate stiffness, respectively. Actuation of the uniaxial plates by removal of the rigid clip reduced the axial stiffness by 97.6%. In comparison with the standard plate, the unactuated uniaxial plate was 58% and 63% stiffer with and without the scaffold, respectively. This indicates a higher degree of stress shielding in the experimental limbs prior to actuation. With the scaffold in place, the effective axial stiffness of the multiaxial and actuated uniaxial plates was increased 9.8- and 10.4-fold, respectively, demonstrating increased axial load transduction to the construct in the compliant plates.

Though comparable to the actuated uniaxial plates in axial compression, the multiaxial plates were an order of magnitude less stiff than either the standard or uniaxial plates in torsion. The torsional stiffness of the multiaxial plates was 95% less than that of the standard plate, while the actuated and unactuated uniaxial plates were 53% and 39% less stiff in torsion, respectively, compared with the standard plates.

While the standard and uniaxial plates had comparable stiffness in response to bending loads, the multiaxial plates were 99.5% less stiff than either the standard or uniaxial plates in bending.

As expected, therefore, mechanical testing revealed that in axial compression, the multiaxial plates and actuated uniaxial plates responded similarly and were significantly less stiff than either the standard plates or the unactuated uniaxial plates. In torsion and bending, the multiaxial plates were substantially less stiff than both the standard and uniaxial plates.

**3.2 Pilot Study 1: Multiaxial Plate.** Following implantation of the multiaxially compliant plates at 8 weeks post-op ($n=2$), the shear and bending loads exerted during ambulation caused large deformations of the defect, resulting in failure of the construct to integrate and eventual nonunion at 12 weeks post-op. (Fig. 2). This indicated that the multiaxially compliant plates were insufficiently stiff to prevent instability of the defect after 8 weeks of stable healing and precluded postmortem CT scanning and biomechanical testing.

**3.3 Pilot study 2: Uniaxial Plate.** As a result of these observations, the compliant plates were redesigned to allow only uniaxial deformations. The rationale was that shear deformations may be responsible for inducing failure, particularly at the scaffold-bone interface. The BMP-2 delivered within PLDL/TCP scaffolds induced formation of low density bone by 4 weeks within the defect region. Longitudinal Faxitron scans demonstrated that after actuation of the plate at week 4 post-op, the uniaxial plate maintained stability of the defect, and both the loaded sample and the contralateral standard control achieved bridging at 12 weeks (Fig. 3).

Quantitative microCT analysis revealed that bone volume (BV) within the central volume of interest was 18.9% greater in the loaded sample (Fig. 4). Consistent with this increase in BV, postmortem biomechanical testing indicated that the torsional strength and stiffness of the loaded construct were substantially greater than those of the contralateral standard control. The torsional stiffness and maximum torque were 25.6- and 3.9-folds greater in the stimulated limb compared with the control (Fig. 5). These properties were greater than those of age-matched intact femurs, whose torsional stiffness and max torque were $0.030 \pm 0.001$ N m/deg and $0.31 \pm 0.02$ N m, respectively, indicating full functional regeneration of that limb. These values were also greater than those previously achieved using the same model with standard fixation and this growth factor dose ([8], unpublished data), suggesting a positive effect of loading on defect healing.

**3.4 Finite Element Modeling.** Image-based finite element modeling of a femur, excised, scanned, and tested at 4 weeks

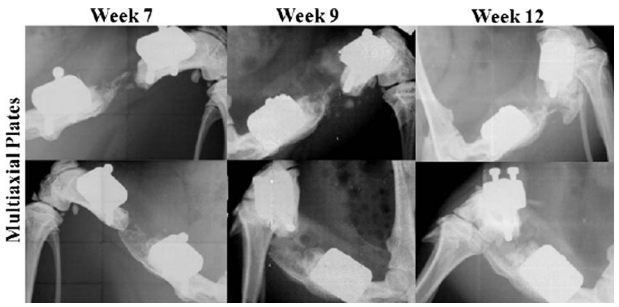


**Fig. 2 Faxitron images of multiaxial plates. Replacement of standard plates with multiaxial plates at 8 weeks post-op resulted in failure under shear and bending loads, which precluded postmortem microCT scanning and biomechanical testing.**

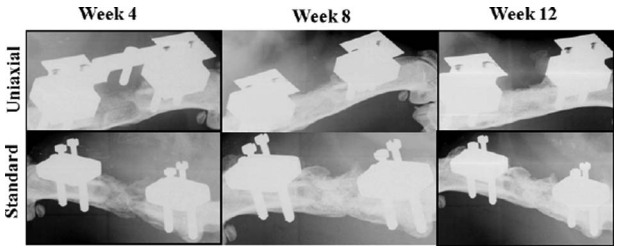


**Fig. 3 Faxitron images of uniaxially compliant plate, actuated at week 4 post-op, and contralateral standard plate. The uniaxially compliant plate successfully maintained stability of the defect over the 12 week implantation period. Both samples achieved qualitative union.**

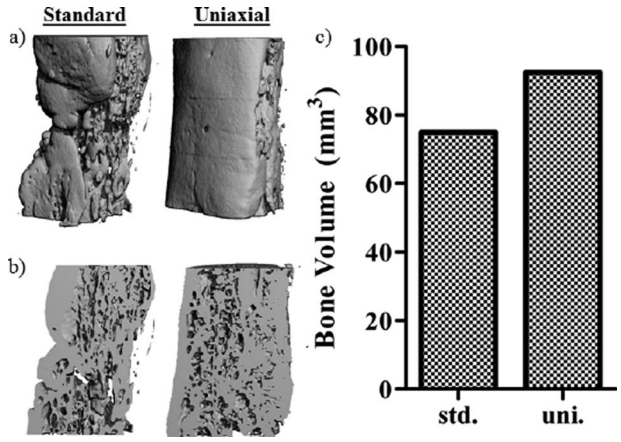


**Fig. 4 Postmortem microCT. (*a*) Images of center (7 mm) used for evaluation, (*b*) sectioned images to demonstrate internal architecture and connectivity, and (*c*) bone volume quantification over a constant VOI. Bone volumes were comparable for the two samples. Cut images demonstrate a more uniformly connected morphology in the uniaxial sample.**

post-op indicated an effective stiffness of 7.05 N/mm. Back calculation of local tissue modulus by comparison of measured to computed effective stiffness indicated an average soft tissue/scaffold modulus of 0.7 MPa. Under estimated physiologic loads, the average axial strain in the newly-formed bone was $-0.09$ $\mu$strain and $-3.8\times10^4$ $\mu$strain in soft tissues/scaffold. FE simulation revealed low principle compressive strains in the ingrowing bone and high strain gradients in the soft tissue adjacent to newly formed bone (Fig. 6). Spatial gradients of strain have previously been postulated to drive local adaptation of bone microstructure during repair [10].

## 4 Discussion

Tissue engineering shows great potential to replace the standard treatments of autograft and allograft for regeneration of large bone defects. The gold standard procedure of using autografted bone is limited by tissue availability, as well as donor-site morbidity. Allograft techniques resolve these issues, but themselves are limited by rejection and problems with integration, revitalization, and remodeling. Bone tissue engineering, therefore, seeks to harness and augment the body's self-restorative potential to limit inflammatory response and promote progenitor differentiation, cell migration, vascular invasion, mineral deposition, and, ultimately, remodeling to normal function, and architecture.

Full defect bridging, construct integration, and eventual scaffold replacement continue to challenge tissue engineers. Limiting

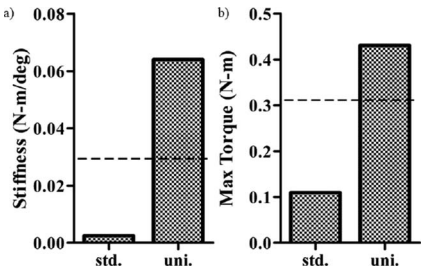


**Fig. 5 Postmortem mechanical testing: (*a*) torsional stiffness and (*b*) maximum torque. Dotted lines represent average properties of age-matched intact femurs. The mechanical properties of the uniaxially loaded sample were 2460% and 293% greater than the sample fixated with the standard plate for stiffness and maximum torque, respectively.**

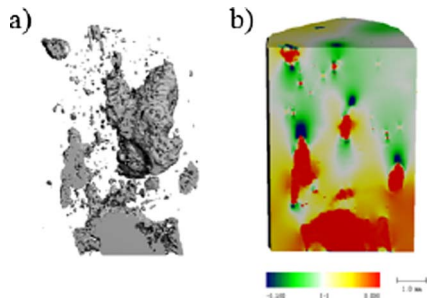


**Fig. 6 Finite element modeling: (*a*) microCT image of bone growth at week 4, sectioned, and (*b*) minimum principle strain distributions at week 4 under estimated boundary conditions at the same section. FE modeling revealed high strain gradients in the soft tissue adjacent to the newly formed bone within the implanted construct.**

factors include nutrient transport, vascular invasion, scaffold degradation kinetics and byproducts, and cell survival and activity. A proper regimen of mechanical loading may positively affect these factors.

Extensive research in the study of mechanotransduction, the mechanism by which a mechanical signal is transduced to a cellular response, has advanced the understanding of the biomolecular mechanisms behind this phenomenon [11]. However, the correlation of stress/strain magnitudes to bone formation remains unknown. Numerous models have been developed to examine the mechanisms by which native bone remodels and adapts to mechanical stimuli [12–19]. The effect of mechanical stimulation on fracture healing is also an area of significant interest, particularly in the formation and healing of a fracture callus [20–27]. Perren and colleagues developed what they term the interfragmentary strain theory, in which the hydrostatic and tensile stress/strain history determines the differentiation of healing tissues [24,28,29].

Research has shown that flexible fixation of bone fractures is more likely to lead to callus healing compared with rigid fixation [26]. This research suggests that mechanical loading can be optimized to accelerate bone formation in a challenging clinical application, and this same effect may be reproduced in tissue-engineered restoration of large bone defects.

Few researchers, however, have examined the effect of mechanical stimulation on tissue-engineered regrowth of bone [30–32]. To that end, a challenging rat segmental defect model has been modified to allow transduction of ambulatory loads to the ingrowing bone within the tissue-engineered construct. Multiaxially compliant fixation plates with low stiffness in response to shear and bending loads failed to maintain defect stability and promote functional repair. The sample fixated with the uniaxially compliant plate allowed axial deformation of the scaffold under physiologic loads, while restricting bending and shear deformations to maintain stability of the defect. Preliminary results using this new in vivo model suggested positive effects of load-bearing on functional defect repair. Loading may influence the functional integration of a tissue-engineered construct by altering the amount, organization, or mineralization of newly formed bone. Upcoming studies will repeat this work with larger sample sizes to test this hypothesis.

## Acknowledgment

This work was supported by the Georgia Tech/Emory Center for the Engineering of Living Tissues (GTEC) NSF Grant No. EEC-9731643 and NIH Grant No. AR051336.

## References

[1] Langer, R., and Vacanti, J. P., 1993, "Tissue Engineering," Science, **260**(5110), pp. 920–926.

[2] Duty, A. O., Oest, M. E., and Guldberg, R. E., 2007, "Cyclic Mechanical Compression Increases Mineralization of Cell-Seeded Polymer Scaffolds In Vivo," J. Biomech. Eng., **129**(4), pp. 531–539.
[3] Robling, A. G., Castillo, A. B., and Turner, C. H., 2006, "Biomechanical and Molecular Regulation of Bone Remodeling," Annu. Rev. Biomed. Eng., **8**, pp. 455–498.
[4] Claes, L. E., Wilke, H. J., Augat, P., Rubenacker, S., and Margevicius, K. J., 1995, "Effect of Dynamization on Gap Healing of Diaphyseal Fractures Under External Fixation," Clin. Biomech. (Bristol, Avon), **10**(5), pp. 227–234.
[5] Goldstein, S. A., 2006, "Tissue Engineering Solutions for Traumatic Bone Loss," J. Am. Acad. Orthop. Surg., **14**(10), pp. S152–156.
[6] Ito, H., Koefoed, M., Tiyapatanaputi, P., Gromov, K., Goater, J. J., Carmouche, J., Zhang, X., Rubery, P. T., Rabinowitz, J., Samulski, R. J., Nakamura, T., Soballe, K., O'Keefe, R. J., Boyce, B. F., and Schwarz, E. M., 2005, "Remodeling of Cortical Bone Allografts Mediated by Adherent rAAV-RANKL and VEGF Gene Therapy," Nat. Med., **11**(3), pp. 291–297.
[7] Lin, A. S., Barrows, T. H., Cartmell, S. H., and Guldberg, R. E., 2003, "Microarchitectural and Mechanical Characterization of Oriented Porous Polymer Scaffolds," Biomaterials, **24**(3), pp. 481–489.
[8] Oest, M. E., Dupont, K. M., Kong, H. J., Mooney, D. J., and Guldberg, R. E., 2007, "Quantitative Assessment of Scaffold and Growth Factor-Mediated Repair of Critically Sized Bone Defects," J. Orthop. Res., **25**(7), pp. 941–950.
[9] Rai, B., Oest, M. E., Dupont, K. M., Ho, K. H., Teoh, S. H., and Guldberg, R. E., 2007, "Combination of Platelet-Rich Plasma With Polycaprolactone-Tricalcium Phosphate Scaffolds for Segmental Bone Defect Repair," J. Biomed. Mater. Res. Part A, **81**(4), pp. 888–899.
[10] Koontz, J. T., Charras, G. T., and Guldberg, R. E., 2001, "A Microstructural Finite Element Simulation of Mechanically Induced Bone Formation," ASME J. Biomech. Eng., **123**(6), pp. 607–612.
[11] Turner, C. H., and Pavalko, F. M., 1998, "Mechanotransduction and Functional Response of the Skeleton to Physical Stress: The Mechanisms and Mechanics of Bone Adaptation," J. Orthop. Sci., **3**(6), pp. 346–355.
[12] Xie, L., Jacobson, J. M., Choi, E. S., Busa, B., Donahue, L. R., Miller, L. M., Rubin, C. T., and Judex, S., 2006, "Low-Level Mechanical Vibrations Can Influence Bone Resorption and Bone Formation in the Growing Skeleton," Bone, **39**(5), pp. 1059–1066.
[13] Kim, C. H., Takai, E., Zhou, H., von Stechow, D., Muller, R., Dempster, D. W., and Guo, X. E., 2003, "Trabecular Bone Response to Mechanical and Parathyroid Hormone Stimulation: The Role of Mechanical Microenvironment," J. Bone Miner. Res., **18**(12), pp. 2116–2125.
[14] Noble, B. S., Peet, N., Stevens, H. Y., Brabbs, A., Mosley, J. R., Reilly, G. C., Reeve, J., Skerry, T. M., and Lanyon, L. E., 2003, "Mechanical Loading: Biphasic Osteocyte Survival and Targeting of Osteoclasts for Bone Destruction in Rat Cortical Bone," Am. J. Physiol.: Cell Physiol., **284**(4), pp. C934–943.
[15] Lanyon, L. E., 1992, "The Success and Failure of the Adaptive Response to Functional Load-Bearing in Averting Bone Fracture," Bone, **13**(2), pp. S17–21.
[16] Lee, K. C., Maxwell, A., and Lanyon, L. E., 2002, "Validation of a Technique for Studying Functional Adaptation of the Mouse Ulna in Response to Mechanical Loading," Bone, **31**(3), pp. 407–412.
[17] Mosley, J. R., and Lanyon, L. E., 1998, "Strain Rate as a Controlling Influence on Adaptive Modeling in Response to Dynamic Loading of the Ulna in Growing Male Rats," Bone, **23**(4), pp. 313–318.
[18] Mosley, J. R., March, B. M., Lynch, J., and Lanyon, L. E., 1997, "Strain Magnitude Related Changes in Whole Bone Architecture in Growing Rats," Bone, **20**(3), pp. 191–198.
[19] Robling, A. G., Burr, D. B., and Turner, C. H., 2000, "Partitioning a Daily Mechanical Stimulus Into Discrete Loading Bouts Improves the Osteogenic Response to Loading," J. Bone Miner. Res., **15**(8), pp. 1596–1602.
[20] Goodship, A. E., and Kenwright, J., 1985, "The Influence of Induced Micromovement Upon the Healing of Experimental Tibial Fractures," J. Bone Joint Surg. Br., **67**(4), pp. 650–655.
[21] Kenwright, J., and Gardner, T., 1998, "Mechanical Influences on Tibial Fracture Healing," Clin. Orthop. Relat. Res., **355**, pp. S179–S190.
[22] Kenwright, J., Richardson, J. B., Cunningham, J. L., White, S. H., Goodship, A. E., Adams, M. A., Magnussen, P. A., and Newman, J. H., 1991, "Axial Movement and Tibial Fractures. A Controlled Randomised Trial of Treatment," J. Bone Joint Surg. Br., **73**(4), pp. 654–659.
[23] Hente, R., Cordey, J., and Perren, S. M., 2003, "In Vivo Measurement of Bending Stiffness in Fracture Healing," Biomed. Eng. Online, **2**, p. 8.
[24] Carter, D. R., Beaupre, G. S., Giori, N. J., and Helms, J. A., 1998, "Mechanobiology of Skeletal Regeneration," Clin. Orthop. Relat. Res., **355**, pp. S41–S55.
[25] Claes, L. E., Heigele, C. A., Neidlinger-Wilke, C., Kaspar, D., Seidl, W., Margevicius, K. J., and Augat, P., 1998, "Effects of Mechanical Factors on the Fracture Healing Process," Clin. Orthop. Relat. Res., **355**, pp. S132–S147.
[26] Augat, P., Margevicius, K., Simon, J., Wolf, S., Suger, G., and Claes, L., 1998, "Local Tissue Properties in Bone Healing: Influence of Size and Stability of the Osteotomy Gap," J. Orthop. Res., **16**(4), pp. 475–481.
[27] Augat, P., Merk, J., Wolf, S., and Claes, L., 2001, "Mechanical Stimulation by External Application of Cyclic Tensile Strains Does Not Effectively Enhance Bone Healing," J. Orthop. Trauma, **15**(1), pp. 54–60.
[28] Perren, S. M., 1979, "Physical and Biological Aspects of Fracture Healing With Special Reference to Internal Fixation," Clin. Orthop. Relat. Res., **138**, pp. 175–196.
[29] Perren, S. M., and Rahn, B. A., 1980, "Biomechanics of Fracture Healing," Can. J. Surg., **23**(3), pp. 228–232.
[30] Guldberg, R. E., Caldwell, N. J., Guo, X. E., Goulet, R. W., Hollister, S. J., and Goldstein, S. A., 1997, "Mechanical Stimulation of Tissue Repair in the Hydraulic Bone Chamber," J. Bone Miner. Res., **12**(8), pp. 1295–1302.
[31] Case, N. D., Duty, A. O., Ratcliffe, A., Muller, R., and Guldberg, R. E., 2003, "Bone Formation on Tissue-Engineered Cartilage Constructs In Vivo: Effects of Chondrocyte Viability and Mechanical Loading," Tissue Eng., **9**(4), pp. 587–596.
[32] Takai, E., Mauck, R. L., Hung, C. T., and Guo, X. E., 2004, "Osteocyte Viability and Regulation of Osteoblast Function in a 3D Trabecular Bone Explant Under Dynamic Hydrostatic Pressure," J. Bone Miner. Res., **19**(9), pp. 1403–1410.